Space-time modelling of blue ling for fisheries stock management

Nicole H. Augustin[1],Verena M. Trenkel[2], Simon N. Wood[1] and Pascal Lorance[2]

[1]Department of Mathematical Sciences, University of Bath, Bath, UK.

[2]Ifremer, rue de l'Ile d'Yeu, BP 21105, 44311 Nantes Cedex 03, France.

nha20@bath.ac.uk.

November 20, 2012

Abstract

Fishery catch data offer a rich potential source of information for management, if modelling can separate out the effects of fishing effort, species behaviour and population abundance. Here we model catch data from the blue ling fishery off the northwest coast of Scotland, using Generalized Additive Mixed Models with a space time interaction represented via a novel tensor product of a soap film smooth of space with a penalized regression spline of time. The use of soap film smoothers avoids imposing correspondences between spatially adjacent areas that are in fact separated by the stock boundary. The comparison of the performance of the soap film smooth for space-time with that of a thin plate regression spline (TPRS) based on root mean squared prediction errors and k-means cross-validation suggests that in this application the former is better overall and in particular for modelling local changes. Further, a model with continuous space-year interaction performed better compared to one with an additive space-year effect. After model selection, checking and validation there is evidence for increasing blue ling abundance from 2000-2010 in some spatial locations.

Keywords: GAMM, finite area smoothing, tensor product smooth, space-time interaction, Tweedie distribution, Molva dypterygia

1 Introduction

Generalised linear models are traditionally used for modelling fisheries catch and effort data to separate fishing strategy, vessel, seasonal and other unwanted effects from population abundance signals which are needed for management (Maunder and Punt, 2004). Continuous spatio-temporal models are rarely used owing to the coarse space-time resolution of the data; hence most studies model space as a categorical variable e.g. Mahevas et al. (2004); Ye and Dennis (2009). In contrast, continuous spatial models have been used for other types of marine data (Augustin et al., 1998; Piet, 2002).

Blue ling has a distinct spatial life history. It occurs on the continental slope and sea mounts to the west off the British Isles and aggregates for spawning in a number of locations situated at bottom depths from about 730 to 1100 m between March and May (Large et al., 2010), from June to February it is more widely distributed at depths from about 200 to 1500m. It is exploited by bottom trawlers all year round (Large et al., 2010). For this study detailed haul-by-haul data for a subset of the fishery were provided by the French fishing industry for the period 2000-2010.

Here we propose Generalised additive mixed models (GAMMs) (Lin and Zhang, 1999; Fahrmeir and Lang, 2001; Wood, 2004, 2006) for modelling space-time variations in haul-by-haul blue ling catches to extract population space-time signals for the whole study area and sub-areas of particular interest, such as spawning locations and individual fishing areas. We are particularly interested in two fisheries management questions:

1. What are the overall trends in blue ling abundance in the whole area, and in each fisheries sub-area from 2000-2010?

2. Is there evidence for a space-time interaction in blue ling abundance suggesting local depletion effects in fishing areas with a longer exploitation history?

These questions are generic to many fish stocks, not just blue ling, and as such our approach to addressing them is also more widely applicable.

To obtain a model sufficiently flexible to adequately represent the data, and to enable investigation of question 2, above, we use a GAMM incorporating a smooth interaction of space and time. GAMMs are appealing for the straightforward way in which smooth effects of covariates can be incorporated alongside the smooth space time effect and random vessel effects. However, our data, like many fisheries datasets, come from a spatially complicated domain where the domain boundary is biologically meaningful: blue ling occurs only within a distinct sea bottom depth range, and the topography of the sea bed is convoluted. When modelling the distribution of blue ling it is important not to assume that densities in geographically neighbouring areas will be similar if these areas are in fact separated by a deeper canyon or have different or untrawlable habitat types. Generically, we should avoid 'smoothing across' boundary features.

This concern is particularly acute when one purpose of the analysis is to look for space-time interactions. Then the model mis-specification inherent in inappropriately imposing smoothness across boundary features can lead to incorrect conclusions in two obvious ways. Suppose that densities change quite sharply across a boundary feature. If model estimation attempts to accommodate this sharp change by increasing the flexibility of the space time smooth, then we will increase the likelihood of concluding that there is a space time interaction even if none is present. Alternatively, if the model estimation incorrectly attributes the sharp change to random variability, resulting in oversmoothing, we will decrease the likelihood of detecting a space time interaction, even when one is present.

In order to ensure that we avoid the possibility of such mis-specification errors, we propose to use space-time smoothers which do not smooth across boundary features. We do this by constructing a novel tensor product smooth from a soap film smooth (Wood et al., 2008) of space and a penalized regression

spline of time. Since the soap film smooth does not smooth across boundary features, then neither will our space-time smooth. The smoother has the advantage of straightforward incorporation into existing GAMM estimation frameworks.

The other major issue for this analysis is model checking. The sampling design of the blue ling catch data is what Diggle et al. (2010) called "preferential sampling" as fishers are trawling in locations and times of the year where they know the target species can be found. However, changing management measures and rising fuel prices in recent years might have modified the spatial fishing strategy. Further, the vessels for which data were available varied in space and time. Changing vessels can influence catches as different vessels have different fishing powers owing to differences in trawl size, engine power or skipper skills (Hilborn and Ledbetter, 1985). Fishers keep a data base of trawlable locations to which they will return repeatedly, thus confounding spatial population and vessel effects. Autocorrelation between successive fishing hauls is created by fishers remaining in productive areas for several hauls, resulting in a data structure of hauls nested within vessels within years (Mikkonen et al., 2008). Given all these effects, it is crucial to appropriately check the spatial and temporal residual structure of the selected model.

Residual analysis is relatively straightforward for uni- or bivariate models, but becomes rather complex for the three dimensional space-time smoothers used here. We propose to check the small scale residual patterns with spatial and temporal variograms. It is common practice to validate selected models by k-fold cross-validation e.g. Yanosky et al. (2008); this has also been suggested for catch data models (Maunder and Punt, 2004). The difficulty in our case is that the spatial and temporal distribution of the data is highly clustered, raising the question of how to divide the data into k-subsets which will each contain enough information on the whole model domain and still back up the spatial structure. We study this question by comparing two sampling schemes, one based on sampling spatial blocks and one based on sampling fishing vessels.

The paper is structured as follows. The next section describes the data and provides results of exploratory analyses. The extension of the soap film smoother to a space-time smoother, the structure of the full model and other methodological issues are presented in Section 3. Results of model fits, validation and comparisons are provided in Section 4. Model checking results are provided as Supplementary Material. Finally we discuss the outcome of the study in terms of the appropriateness of the modelling approach, and the answers to the principle fisheries management questions given above.

2 The data and some exploratory analysis

The data contains information on selected fishing hauls from 20 French deep-sea trawlers operating in the Northeast Atlantic during the period 2000-2010. For each haul location (latitude and longitude), year, month, day, mean fishing depth, haul duration (a proxy for fishing effort) and landings (biomass in kg) by species are reported. For each vessel engine power (kWatt) is also available. The data come from volunteer vessels for which information for all hauls during a given period was provided (see description in Lorance et al. (2010)). The participation of vessels varied over the years as some were decommissioned or moved to other fisheries and new vessels were built. The data was restricted to hauls with haul duration between 30 and 600 mins and haul depth between 200 and 1100m as this depth range encompasses the core distribution of blue ling and allows removal of fishing hauls targetting other species such as roundnose grenadier; deeper hauls contained generally no blue ling. The limits of the study area were defined roughly following depth contours leading to an irregular shaped area with a deeper canyon at latitude 60 without blue ling separating suitable areas in the North from those further South (Figure 1). The two small extrusions between latitude 56 and 58 correspond to two seamounts. Data from outside this area were removed leading to 17614 hauls in the data set. Note that hauls were not evenly distributed within the study area and no information was available for certain locations in certain years (Figure 1).

Further, although each vessel operated in a more or less restricted area, which sometimes varied over the years, different vessel pairs overlapped in certain areas at certain times, giving a chance to separate vessel effects from space-time effects.

As expected due to the seasonal movements of blue ling, monthly median catch per hour varied strongly on a seasonal basis but also between years (Figure 2). Zero landings indicate absence or very low abundance of blue ling, i.e. catch less than one 25 kg box, in the location at the time. The data contained 17% of zero hauls which were located throughout the study area and found in all years.

For prediction purposes we used the same five fishing areas as Lorance et al. (2010) (coloured areas in 2009 in Figure 1). The areas have different fishing histories, with area new5 and new6 having only been exploited since 2000 and the other three since the 1990s. Time trends in these areas will be investigated to answer the question of the impact of the fishing history on local time trends. Predictions for the two (Rosemary and Edge) of the five spawning areas identified by Large et al. (2010) and listed as special protection areas for blue ling in Regulation (EC) No.43/2009 provide insight into long term stock depletion (orange and yellow areas in 2010 in Figure 1).

3 Methodology

3.1 The Model

The response 'kg blue ling in haul i' (y_i) is modelled using a generalised additive mixed model (GAMM) (Lin and Zhang, 1999; Fahrmeir and Lang, 2001; Wood, 2004, 2006), as follows.

$$\begin{aligned}\log(\mu_i) = {} & f_1(\texttt{duration}_i) + f_2(\texttt{depth}_i, \texttt{year}_i) + v_{k(i)} \\ & + f_3(\texttt{depth}_i) + f_4(\texttt{month}_i) + f_5(\texttt{depth}_i, \texttt{month}_i) + f_6(\texttt{north}_i, \texttt{east}_i, \texttt{year}_i),\end{aligned} \tag{1}$$

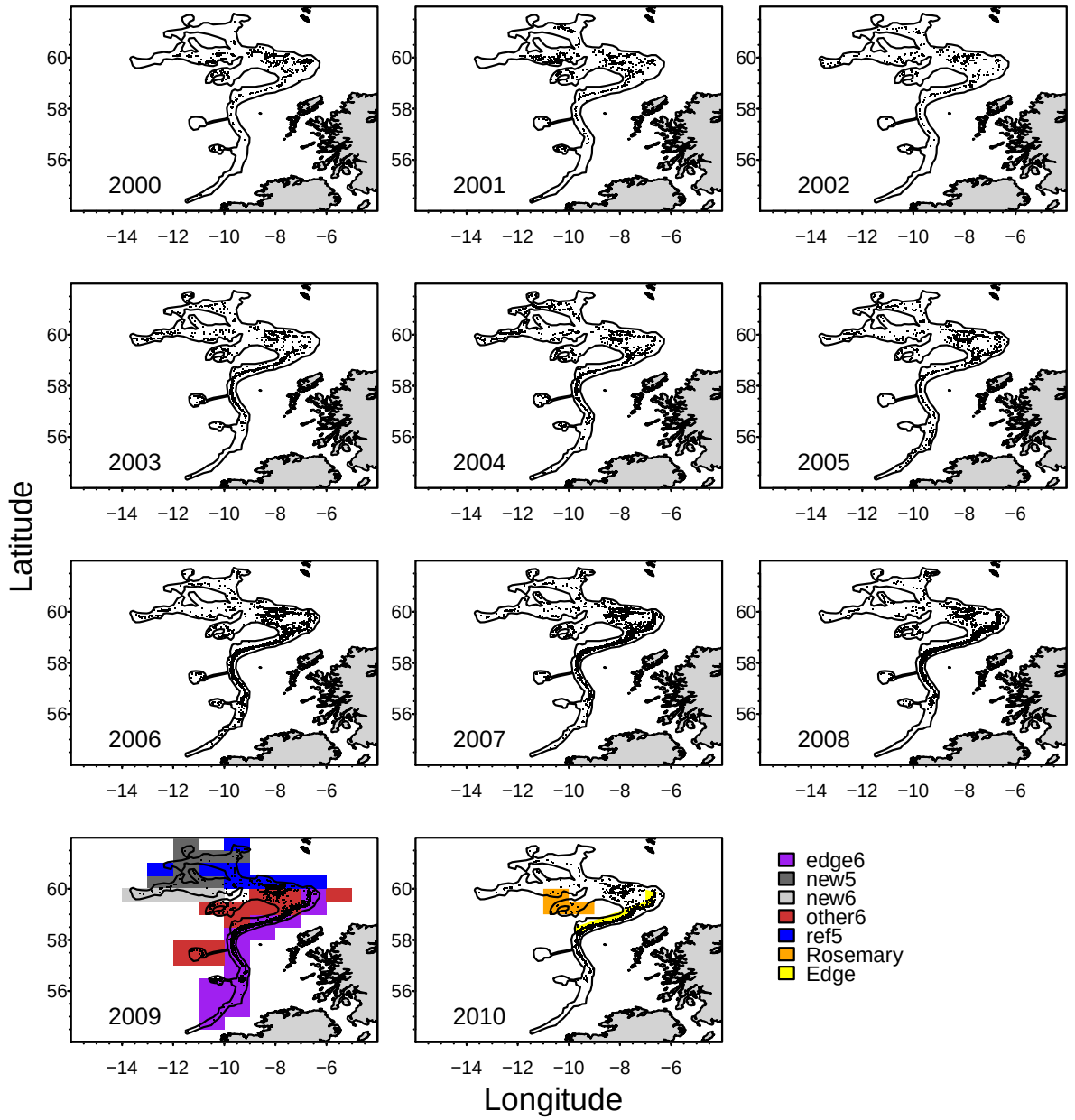

Figure 1: Position of hauls per year. The contour line indicates the boundary used in the soap film smoother. In 2009 the areas shaded in different colours denote areas with different fishing histories. In 2010 the spawning areas are shaded in orange and yellow.

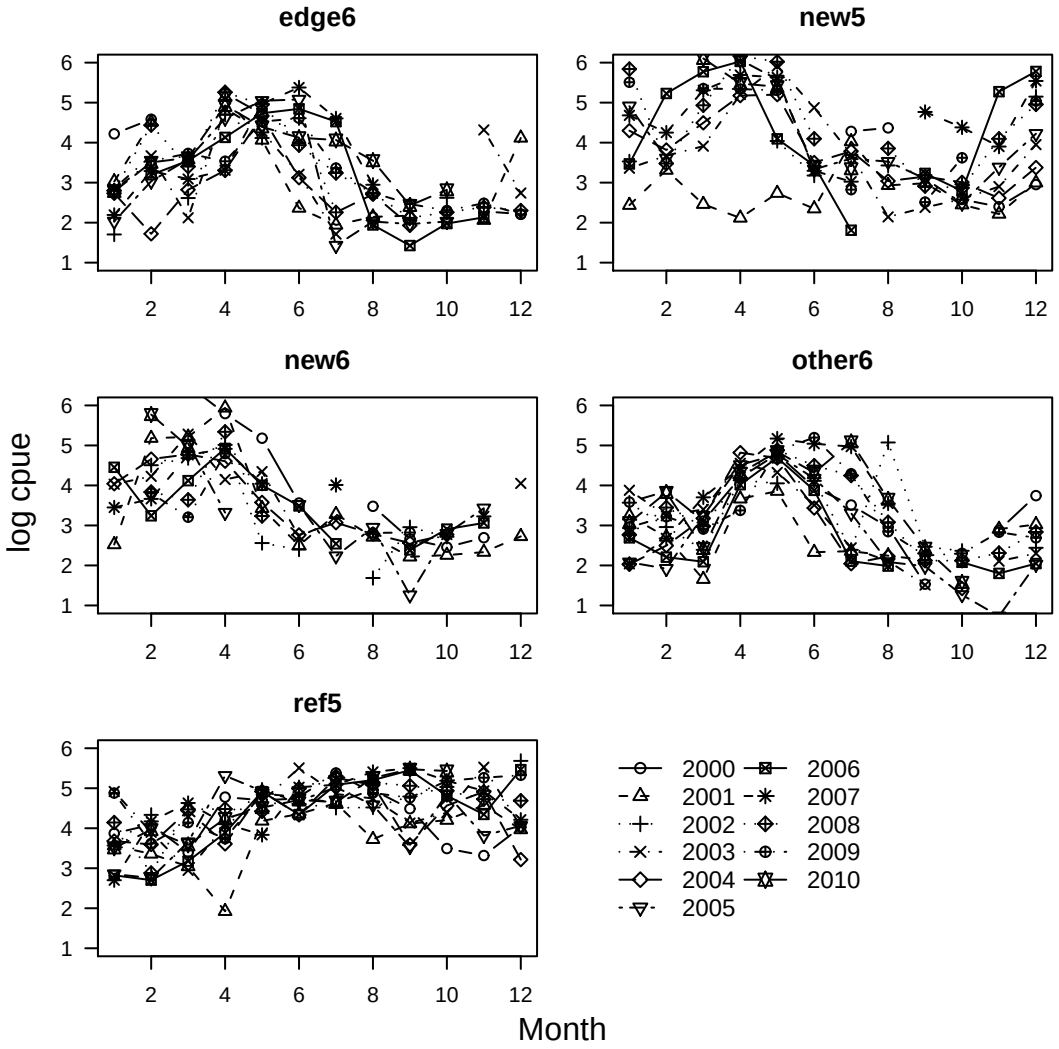

Figure 2: Observed monthly median catch per hour by year and area. On the y axis the log median catch (log kg) per hour is shown.

where $\mu_i = E(y_i)$ and y_i is from a Tweedie distribution (Dunn and Smith, 2005; Tweedie, 1984) with variance $\phi\mu_i^p$. The Tweedie distribution was chosen here as it can handle continuous data with many zeros. $k(i)$ indexes the vessel that made the i^{th} haul and f_{1-6} are smooth functions of the covariates available with each haul: haul `duration`, sea bottom `depth`, `year`, `month` and location as `lat`itude, `lon`gitude. The geographic coordinates `north`ing and `east`ing are longitude and latitude projected

onto a square grid using the universal transverse mercator projection. $v_{k(i)}$ is a random vessel effect, assumed i.i.d. $N(0, \sigma_v^2)$. We also considered a variant of the model in which the vessel random effect is replaced by a linear function, f_7, of vessel engine `power`. The Tweedie index parameter p was set to 1.5 as this maximized the penalized log-likelihood for all model variants discussed below.

f_1 and f_3 are represented using thin plate regression splines (TPRS); f_4 is represented using a cyclic cubic regression spline (CCRS). Turning to the interaction terms, f_2 is a tensor product of a TPRS and cubic regression spline (CRS) and f_5 is a tensor product of a TPRS and a CCRS. The interaction f_2 is required because if local depletion has taken place the effect of depth may change over years. f_5 accounts for the fact that during the spawning season blue ling aggregate at a certain depth, and hence we expect the effect of depth to change by season.

The three dimensional smooth $f_6(\texttt{north}_i, \texttt{east}_i, \texttt{year}_i)$ is a tensor product of a two-dimensional isotropic smoother for space and a one dimensional CRS smooth for year (we used month and year separately as covariates in order to separate the strong seasonal effect from the long term trend). The tensor product construction allows f_6 to be isotropic in space while being invariant to the relative scaling of space and time. This invariance is important, since there is no 'natural' scaling of space against time in this setting, and we do not want the modelling results to depend on an arbitrary choice in this regard (Augustin et al., 2009).

For the isotropic marginal smooth of space we will compare the performance of a soap film smooth (Wood et al., 2008) with a TPRS (Wood, 2006). Both these marginal smooths are isotropic, but the soap film basis also respects the biological boundary of blue ling, whereas the TPRS will smooth across areas such as the two small extrusions at latitude 56 and 58 corresponding to seamounts.

Since the tensor product construction involving a soap film smooth is novel and non-standard, we present it in detail here. For notational compactness we write `n` for `north`, `e` for `east` and `y` for `year`, in the

rest of this section (and remark that we use n and e co-ordinates on a 'nearly square' grid, rather than using latitude and longitude). We start with the two *marginal* bases and penalties for y and n, e. The marginal basis for year can be of any type, e.g. a CRS:

$$f_y(\mathtt{y}) = \sum_{i=1}^{P} \alpha_i a_i(\mathtt{y}),$$

where α_i are parameters while a_i are basis functions.

The marginal basis for space (n, e) is a soap film basis as described in Wood et al. (2008). Soap film smoothers are finite area smoothers, constructed by imagining the value of the smooth on the area boundary as defining the 'height' of a wire loop running around the boundary. This loop is dipped in a soap solution to obtain a 'completely smooth' soap film over the finite area of interest, and this film is then allowed to distort vertically in a smooth manner in order to approximate any smooth function over the domain. Usually both the boundary height and interior distortion are estimated from data. These smoothers are subject to two penalties (one for the boundary and one for the interior), which makes tensor product construction non standard. The key to making progress is to notice that the soap film, $f_{n,e}$, can be written as the sum of two singly penalized smooth components

$$f_{n,e}(\mathtt{n},\mathtt{e}) = f^b_{n,e}(\mathtt{n},\mathtt{e}) + f^w_{n,e}(\mathtt{n},\mathtt{e}) = \sum_{l=1}^{L} \delta_l d_l(\mathtt{n},\mathtt{e}) + \sum_{k=1}^{K} \gamma_k g_k(\mathtt{n},\mathtt{e}).$$

The first component $f^b_{n,e}$ (corresponding to the first summation) represents the boundary interpolating soap film with parameters δ_l and basis functions d_l. The second term $f^w_{n,e}$ represents the smooth distortion from the boundary interpolating film and has parameters γ_k and basis functions g_k. Note that $f^w_{n,e}$ and the g_k are zero on the boundary of the area. For the technical details of constructing a soap film smooth we refer to Wood et al. (2008).

For converting the smooth function f_y into a smooth function of n and e we let the temporal smooth f_y vary smoothly with the spatial dimensions n and e. This can be achieved by letting its parameters vary

with $\mathtt{n}$ and $\mathtt{e}$. Using the soap basis setup for $f_{n,e}$ we can write:

$$\alpha_i(\mathtt{n},\mathtt{e}) = \sum_{l=1}^{L} \delta_{il} d_l(\mathtt{n},\mathtt{e}) + \sum_{k=1}^{K} \gamma_{ik} g_k(\mathtt{n},\mathtt{e})$$

which results in the space time smooth function

$$\begin{aligned} f_{y,n,e}(\mathtt{y},\mathtt{n},\mathtt{e}) &= f^b_{y,n,e}(\mathtt{y},\mathtt{n},\mathtt{e}) + f^w_{y,n,e}(\mathtt{y},\mathtt{n},\mathtt{e}) \\ &= \sum_{i=1}^{P}\sum_{l=1}^{L} \delta_{il} d_l(\mathtt{n},\mathtt{e}) a_i(\mathtt{y}) + \sum_{i=1}^{P}\sum_{k=1}^{K} \gamma_{ik} g_k(\mathtt{n},\mathtt{e}) a_i(\mathtt{y}), \end{aligned}$$

where $f^b_{y,n,e}$ is the time varying boundary interpolating soap film and $f^w_{y,n,e}$ is the time varying distortion of the film. Note that we would obtain exactly the same result by using the marginal smooth of $\mathtt{y}$ to allow the coefficients of the spatial smoother to become functions of year, $\delta_l(\mathtt{y})$ and $\gamma_k(\mathtt{y})$.

Having obtained a tensor product basis, we also require penalties on the smooth which will maintain the space-time scaling invariance inherent in the basis. Again the penalties can be constructed from the penalties of the marginal smooths. In particular, suppose that each smooth has an associated functional, J, that measures its roughness and can be written as a quadratic form in its coefficients. The J obviously depends on the basis function type. For the marginal temporal smooth f_y it is the CRS penalty:

$$J_y(f_y) = \boldsymbol{\alpha}^T \mathbf{S}_y \boldsymbol{\alpha} = \int f''_y(\mathtt{y})^2 d\mathtt{y}$$

There are two penalties relating to the spatial soap smooth. For the boundary-interpolating-film, $f^b_{n,e}$, the penalty is a measure of boundary wiggliness. Let $n(r), e(r)$ define the path around the boundary of the study area parameterized in terms of distance around the boundary, B, (from an arbitrary start point)

$$J^b_{n,e}(f_{n,e}) = \boldsymbol{\delta}^T \mathbf{S}^b_{n,e} \boldsymbol{\delta} = \int_B \left(\frac{\mathrm{d}^2 f^b_{n,e}(n(r),e(r))}{\mathrm{d}r^2} \right)^2 dr.$$

For the deviation-from-film smoother:

$$J^w_{n,e}(f_{n,e}) = \boldsymbol{\gamma}^T \mathbf{S}^w_{n,e} \boldsymbol{\gamma} = \int_\Omega \left(\frac{\partial^2 f^w_{n,e}}{\partial \mathtt{n}^2} + \frac{\partial f^w_{n,e}}{\partial \mathtt{e}^2} \right)^2 d\mathtt{n} d\mathtt{e}$$

where Ω is the region made up of all locations within the boundary B. Note that in the last three equations the matrices $\mathbf{S}_y$, $\mathbf{S}^b_{n,e}$ and $\mathbf{S}^w_{n,e}$ contain known coefficients and the vectors $\boldsymbol{\alpha}$, $\boldsymbol{\delta}$ and $\boldsymbol{\gamma}$ contain the parameters of the respective marginal smooths.

To obtain an overall penalty we apply the penalties of the spatial smooth to the spatially varying coefficients of the marginal temporal smooth, $\alpha_i(\mathtt{n}, \mathtt{e})$, resulting in

$$\sum_i^P J^b_{n,e}(\alpha_i), \text{ and } \sum_i^P J^w_{n,e}(\alpha_i).$$

Equivalently we can apply the penalty of the temporal smooth to the coefficients of the marginal spatial smooth, considered as functions of time, $\delta_l(\mathtt{y})$ and $\gamma_k(\mathtt{y})$, yielding,

$$\sum_l^L J_y(\delta_l) \text{and} \sum_k^K J_y(\gamma_k).$$

Hence the wiggliness of $f_{y,n,e}$ can be measured by the sum of 4 penalties each weighted by a smoothing parameter ($\lambda_\cdot$),

$$J(f_{y,n,e}) = \lambda^b_{n,e} \sum_i^P J^b_{n,e}(\alpha_i) + \lambda^w_{n,e} \sum_i^P J^w_{n,e}(\alpha_i) + \lambda^\delta_y \sum_l^L J_y(\delta_l) + \lambda^\gamma_y \sum_k^K J_y(\gamma_k) \tag{2}$$

3.2 Parameter estimation

The GAMM in equation 1 can be expressed as a generalized linear mixed model (GLMM):

$$\log(\mu_i) = \mathbf{X}_i \boldsymbol{\theta} \tag{3}$$

where $\mathbf{X}_i$ is a row of the model matrix containing all components of the model. That is all strictly parametric components, such as explanatory variables of linear effects, dummy variables for the random effects and all the basis functions evaluated at observations i. The parameter vector $\boldsymbol{\theta}$ contains the coefficients of linear terms, the random vessel effects and the bases.

We estimate parameters with a nested iteration scheme of penalised iteratively re-weighted least squares (PIRLS, see for example Wood (2006)) and approximate restricted maximum likelihood (REML) es-

timation of the smoothness parameters as described in Wood (2011). The outer iteration updates the smoothness parameters by minimising a Laplace approximation of the REML where $\boldsymbol{\theta}$, the parameter vector with the coefficients of linear terms, the random vessel effects and the bases, is integrated out and with each iteration step an inner PIRLS iteration is carried out to find $\hat{\boldsymbol{\theta}}$. This scheme is implemented in the gam() function of the mgcv R package. It is worth noting that the penalised likelihood treats random effects as penalised fixed effects and the effective degrees of freedom include also the degrees of freedom for the random (vessel) effect. We estimate temporal trends with Bayesian credible intervals by sampling from the posterior of $\boldsymbol{\theta}$ to obtain a sample from the predictive distribution of the response (Wahba, 1983; Silverman, 1985; Wood, 2006). For this, model 3 is represented as a Bayesian model, where the smooth terms are a mixture of fixed and random effects. This approach recognises that imposing a particular penalty effectively imposes some prior beliefs about the likely characteristics of the correct model. That is, the model structure allows considerably more flexibility than is believed to be really likely, and the choice is made to penalize models that are in some sense too wiggly. This is done by specifying a prior distribution on the parameters $\boldsymbol{\theta}$, with $f_\theta(\boldsymbol{\theta}) \propto \exp(-\frac{1}{2}\boldsymbol{\theta}^T \sum_{i=1}^{4} \mathbf{S}_i \tau_i \boldsymbol{\theta})$, where τ_i are parameters controlling the dispersion of the prior and the matrices $\mathbf{S}_i$ contain known coefficients of the 4 penalties of $J(f_{y,n,e})$ in equation 2. Choosing the τ_i in this Bayesian formulation is equivalent to choosing the smoothing parameters λ_i. Here the choice of the λ_i is data driven as they are estimated by REML. With the generally improper prior distribution for $\boldsymbol{\theta}$ a posterior distribution for $\boldsymbol{\theta}$ can be derived, see Wood (2006) for details. The Bayesian posterior covariance matrix of the parameter vector $\boldsymbol{\theta}$ (with the coefficients of linear terms, the random vessel effects and the bases) can then be used to obtain Bayesian credible intervals. This is done by repeatedly sampling parameter vectors from a multivariate normal distribution where the mean is the estimated parameter vector $\hat{\boldsymbol{\theta}}$ and the variance matrix is the Bayesian posterior covariance matrix. From the sampled parameter vectors we obtain samples of fitted values, i.e. the predictive distribution, by multiplying the model matrix with each sample parameter

vector. We estimate the temporal trend per area for each sample of fitted values by averaging over all locations by area. The median, 2.5% and 97.5% percentile of the distribution of temporal trends are the required summary statistics for the time trends displayed with 95% Bayesian credible intervals.

Example R code is supplied as Supplementary Material on the journal web page.

3.3 Model selection and validation

Our model selection strategy is that we start with the full model (eq. 1, model 1a) and then check whether it can be simplified (Table 1). First, we check whether the random vessel effect can be replaced by an linear effect of vessel power (model 2a). Then we check whether the model can be simplified by replacing the three dimensional space-time effect by an additive space-time effect (model 3a and 4a). Finally we check whether the relatively complicated soap film smoother is required for the spatial effect, or whether the same model fit can be achieved by using a thin-plate regression spline basis for the spatial dimension instead (models 1b, 2b, 3b and 4b). These models used a basis dimension equivalent to the soap smooth basis dimension of model 1a - 4a.

For model checking and investigating whether the final selected model has eliminated spatial and temporal correlation in residuals we use two types of semi-variograms. For the first type we estimate empirical semi-variograms per vessel along the time axis (in days) for checking if there was any spatial and temporal correlation present in the residuals within a vessel. For the second type we estimate semi-variograms in space by year over all vessels for the spawning and non-spawning season. For each variogram envelops representing minimum and maximum values derived by permuting data points between locations respectively times were created using the geoR package in R (Ribeiro Jr. and Diggle, 2001). These variograms indicate model mis-specification in terms of space and time if the empirical points lie outside the envelops.

Given the complex nature of the problem and the fact that there is potential unexplained spatio-temporal correlation in residuals we base model selection on a the root mean squared prediction error (RMSPE), which is independent of the likelihood. We estimate the RMSPE by k-fold cross-validation. As the spatial and temporal distribution of the data is highly clustered, we compare two sampling schemes for the cross-validation, one based on randomly sampling rectangles of 1 degree longitude and 1/2 degree latitude (as shown on Figure 1) within year (scheme R) and one based on randomly sampling fishing vessels within year (scheme *V*). Thus we split the observed space-time data into $K = 11$ sets of similar size where each set contains a random rectangle by year selection (scheme *R*) or a random vessel by year selection (scheme*V*). In turn, data of one of the 11 sets are left out, the model is fitted to the remaining data and predictions, $\hat{y_i^c}$, where i is the index of observation 1 to 17614, are obtained at the space-time locations of the omitted set. The RMSPE is then calculated as $RMSPE = \sqrt{\frac{\sum_{i=1}^{n}(y_i - \hat{y}_i)^2}{n}}$. For the cross-validation RMSPE $\hat{y}_i$ is replaced with $\hat{y}_i^c$.

4 Results

4.1 Model selection and validation

The estimates of the RMSPE were in the same order, independent of whether the random rectangle by year selection (scheme *R*) or a random vessel by year selection (scheme*V*) was used. The comparison of the full model (Model 1a) with the model where the vessel random effect was replaced by a linear function of vessel power (Model 2a) as a proxy for fishing performance showed that vessel power (Model 2a) seemed to be sufficient for explaining differences between vessels (Table 2). Considering individual fishing areas, model 2a has a reduced RMSPE for two out the five areas.

Moving on to testing whether the model can be simplified, shows that both models 3a and 4a had larger overall RMSPE values compared to the models with space-time interaction (models 1a and 2a). Looking

Table 1: Model definitions. Soap: soap smoother; TPRS: thin-plate regression spline.

Model (number)	Terms	Spatial smoother
Base	$f_1(duration_i) + f_2(depth_i, year_i)$ $+f_3(depth_i) + f_4(month_i) + f_5(depth_i, month_i)$	–
Full.ves (1a)	Base $+v_{k(i)} + f_6(north_i, east_i, year_i)$	soap
Full.pow (2a)	Base $+\beta power_{k(i)} + f_6(north_i, east_i, year_i)$	soap
Add.ves (3a)	Base $+v_{k(i)} + f_7(north_i, east_i) + f_8(year_i)$	soap
Add.pow (4a)	Base $+\beta power_{k(i)} + f_7(north_i, east_i) + f_8(year_i)$	soap
Nosoap.full.ves (1b)	Base $+v_{k(i)} + f_9(north_i, east_i, year_i)$	TPRS
Nosoap.full.pow (2b)	Base $+\beta power_{k(i)} + f_9(north_i, east_i, year_i)$	TPRS
Nosoap.add.ves (3b)	Base $+v_{k(i)} + f_{10}(north_i, east_i) + f_{11}(year_i)$	TPRS
Nosoap.add.pow (4b)	Base $+\beta power_{k(i)} + f_{10}(north_i, east_i) + f_{11}(year_i)$	TPRS

again at individual areas, models with additive space and time had smaller RMSPE for three areas.

Finally, we checked whether the soap smoother is required. This question is investigated by comparing the fits of the models with soap smooth which were best in terms of RMSPE (Model 1a & 2a) and with a TPRS (Model 1b & 2b) (Table 2). For the models with vessel power, the RMSPE is in favour of the model with the soap smoother (Model 1b). When treating vessel as a random effect the cross-validation RMSPE is similar for the soap and TPRS smoothers (Model 1a & 1b). For completeness we have also fitted the additive space-time model with a tensor product where a TPRS is used for that spatial dimension (model 3b & 4b in Table 2); model 3b has overall the largest RMSPE.

As model 2a had the smallest overall RMPSE and for four out of six areas models with soap film smoother were best in terms of RMSPE, model 2a with the space-time interaction modelled by the extended soap film smoother and using vessel power was selected as the best model.

The model fit was adequate for all models and the model checking results presented in the Supplementary Material showed that the residuals plots were qualitatively similar for all considered models.

4.2 Interpretation of model results

A strong seasonal pattern was found with peak catches in summer (Figure 3 left). The month effect varied with depth, indicating that spawning aggregations with higher densities in April-May were fished at depths between 700 and 900m and at slightly shallower depths up to June (Figure 3 right). The main depth effect was a flat function with depth, which varied little across years (not shown). The spatial distribution showed some localised hot spots and generally higher values in the Northern part (Figure 4). This figure also illustrates the overspill that happens when an ordinary tensor product smooth (model 3b) is used, as the model smoothed across fine scale patterns in the North.

The overall time trend of mean haul landings in kg was predicted by fishing area for January in each year

Table 2: Model statistics and 11-fold cross validation results. Effective degrees of freedom (edf) and root mean squared prediction error (RMSPE) for cross-validation predictions. Cross-validation sampling scheme: random vessel-year selection (^{V}), random spatial units-year selection (^{R}).

Model (number)	edf	RMSPE^R	RMSPE^V	RMSPE^R				
		overall	overall	edge6	new5	new6	other6	ref5
Full.ves (1a)	335.98	699.43	705.08	431.73	1115.22	**843.57**	445.87	1065.99
Full.pow (2a)	319.15	**695.80**	**702.42**	436.08	1078.32	849.82	446.02	**1063.30**
Add.ves (3a)	208.95	711.04	705.13	427.55	1080.71	875.78	426.98	1121.14
Add.pow (4a)	210.17	708.33	702.78	430.64	**1062.11**	883.37	426.82	1115.93
Nosoap.full.ves (1b)	376.23	700.13	705.28	425.99	1132.29	855.42	431.43	1073.31
Nosoap.full.pow (2b)	362.44	697.49	704.74	430.17	1100.65	860.24	431.53	1071.76
Nosoap.add.ves (3b)	218.68	707.61	704.78	**424.50**	1087.72	880.94	423.22	1111.81
Nosoap.add.pow (4b)	202.19	705.45	703.71	427.74	1074.07	886.84	**423.05**	1106.74

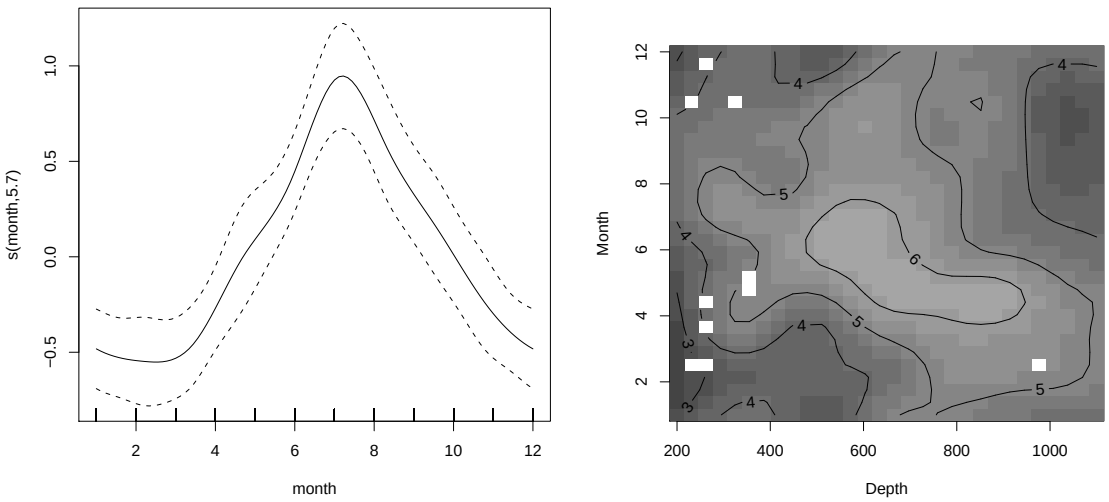

Figure 3: Fitted model smooths for model 2a (soap smoother). Month smooth with $\pm$ two standard errors (left); Depth-month smooth (right).

using the best model 2a with a median haul duration of 6 hours, a median depth of 850 m and a median vessel power of 1850 kWatt. For spawning areas predictions were made for the peak of the spawning period (April). All predicted time trends were slightly to substantially increasing over the study period 2000-2010 (Figure 5). Area edge6 and other6 which together with ref5 have the longest exploitation history, had the lowest predictions and the narrowest prediction intervals. In contrast, the predictions for the two spawning areas Rosemary and Edge were much higher with both increasing trends in recent years.

5 Discussion

We have used GAMMs for modelling space-time fishery catch data. GAMMs are a flexible framework which allows for smooth effects of covariates, caters for a spatially complicated domain boundary, and multi-dimensional functions of covariates and space and time. In other application contexts, such as

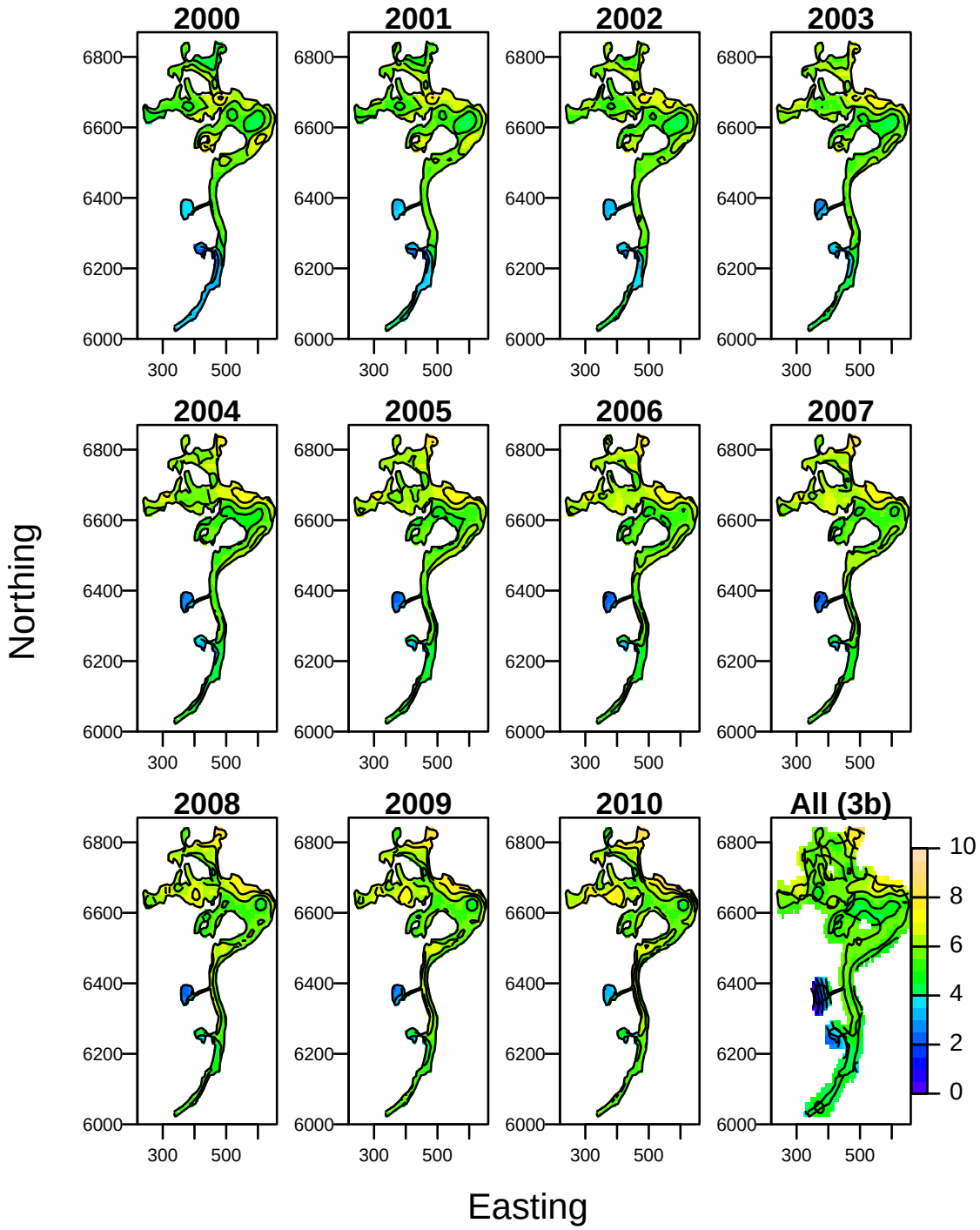

Figure 4: Fitted spatial model smooths by year for model 2a (soap smoother) and model 3b (TPRS smoother).

repeated observations of weather station data, the use of spatio-temporal dynamic models or state-space model have been proposed by Gelfand et al. (2005), Stroud et al. (2001), Strickland et al. (2011) and others.

The two dimensional soap smoother proposed by Wood et al. (2008) was extended to three dimensions using tensor products. This three dimensional tensor product allowed us to account for the complex domain boundary of blue ling which is driven by the topography of the sea bed. Hence we could check whether a space-time interaction is present in blue ling abundance while being certain of not over- or underfitting due to having to smooth across spatial boundaries. The best model in terms of RMPE estimated by 11-fold crossvalidation had a space-time interaction term. This answers the fisheries management questions posed in the introduction. Predicted relative blue ling population time trends were slightly increasing in all five fishing and both spawning areas during the period 2000-2010, providing no evidence for recent local depletion caused by fishing. However, predicted densities in two of the three areas with the longest fishing history, edge6 and other6 were much lower compared to the other areas and the increasing time trends were very small indeed. These two areas are closest to the Scottish fishing ports used by the French vessels. Thus decreasing quotas and increasing fuel prices might have moved the fleet away from ref5 but maintained it in edge6 and other6.

Comparing the soap smoother basis with the TPRS basis for the spatial dimension of the space-time smooth showed that overall, the soap smoother performed better in terms of RMSPE, although differences in absolute terms were small. The soap film basis has the clear advantage that it respects the natural boundary, which in this case depends on bathymetry. The disadvantage is that it relies on manual knot placement and results can be sensitive to knot placements. In comparison using a TPRS as a basis for the spatial dimension, does not respect a natural boundary but is at the same time easier to use because it does not require the knot placement. Both type of basis function have the isotropy property, i.e. the

smoothness is uniform in any geographic direction.

The blue ling data posed several challenges for model checking and validation due to its unbalanced, spatially clustered and preferential nature. We have no means of assessing how biased our estimates are in absolute terms, since no non-preferential survey data are available. However, our model controls for effects of fisheries management and targeting by the inclusion of the terms $\beta\texttt{power}_{k(i)} + f_1(\texttt{duration}_i) + f_2(\texttt{depth}_i, \texttt{year}_i) + f_5(\texttt{depth}_i, \texttt{month}_i)$, and for predicting relative time trends we are able to control for vessel power, month and depth.

Two sampling schemes were compared for the 11-fold cross-validation, one based on sampling spatial blocks and one based on sampling fishing vessels. The first scheme gave for all models smaller estimates of prediction error, but overall it did not make much difference which sampling scheme was used. Thus the model cross-validation results were robust to the sampling scheme used despite the highly clustered nature of the data.

The selected model was successful in explaining variability in the data (adjusted R^2=0.41) compared to other catch per unit effort (CPUE) standardisations studies. For example, only 13-21% deviance explained was achieved for the Australian shark fishery (Punt et al., 2000). The high goodness-of-fit of this study contradicts the opinion of Maunder and Punt (2004) that for highly disaggregated (haul by haul) data as used here, explanatory model power would be expected to be low and data would need to be aggregated to reduce variability and increase model goodness-of-fit. The good model fit is a reflection of the use of flexible non-linear multi-dimensional functions of appropriate explanatory variables combined with the Tweedie distribution for these highly skewed CPUE data. Indeed, depth was an important variable for explaining inter-haul variability of blue ling catches. In contrast, using a continuous model for space did not substantially increase model fit compared to a simpler model fitted to a subset of the data which treated space as discrete units (blocks of 1 degree latitude by 0.5 degree longitude) and had

a year-area interaction term (Lorance et al., 2010). However, with the continuous space model it was straighforward to produce time trends for the whole area or any sub-area as desired, for example the two spawning areas.

Finally, engine power was found to be sufficient for accounting for vessel effects. This is not surprising as blue ling are fished on the continental slope primarily at depths around 700 m which are rather difficult conditions for trawling and hence engine power is likely to be the primary determinant of vessel fishing power and size of the trawl that can be towed.

Example R code and results on model checking are provided as Supplementary material for this article, available online at the journal's website.

Acknowledgements

We thank the producers organisation PROMA/PMA and the fishing company EURONOR for providing access to their tallybooks. This study has been carried out with financial support from the Commission of the European Communities, project DEEPFISHMAN, Grant agreement no. 227390.

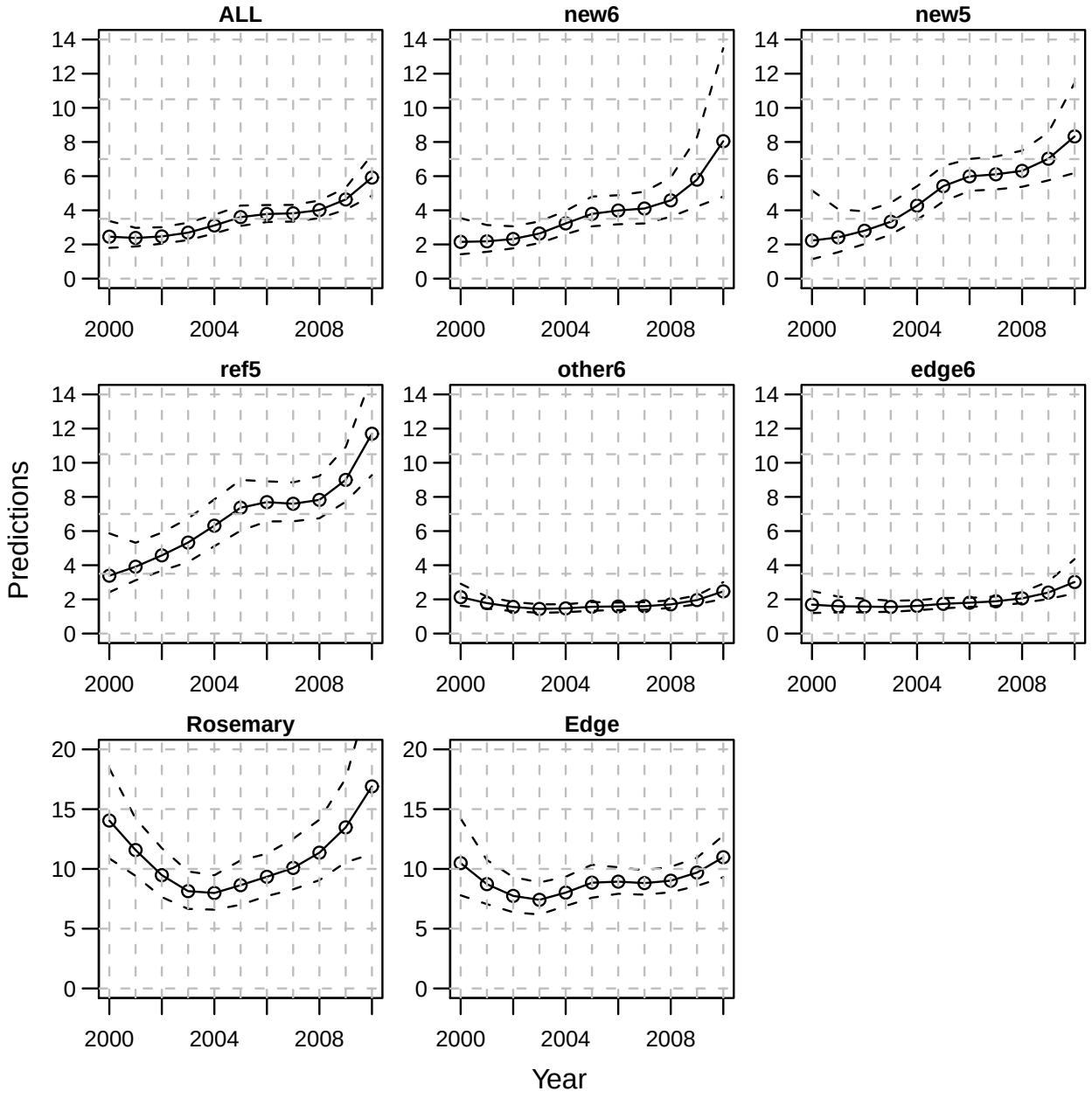

Figure 5: Time trends of median haul landings in 100 kg by area (ALL areas, new6, new5, ref5, other6 and edge6) and for two spawning areas (April) predicted with the selected model (model 2a). Time trends were predicted by fishing area for January in each year for a haul duration of 6 hours, a depth of 850 m and a vessel power of 1850 kWatt. For spawning areas predictions were made for the peak of the spawning period (April) and otherwise with the same fixed values as the other predictions. The dashed lines are 95% Bayesian credible intervals.

References

Augustin, N. H., Borchers, D. L., Clarke, E. D., Buckland, S. T., and Walsh, M. (1998). Spatiotemporal modelling for the annual egg production method of stock assessment using generalized additive models. *Can. J. Fish. Aquat. Sci.*, 55:2608–2621.

Augustin, N. H., Musio, M., von Wilpert, K., Kublin, E., Wood, S. N., and Schumacher, M. (2009). Modelling spatio-temporal forest health monitoring data. *J. Am. Statist. Ass.*, 104(487):899–911.

Diggle, P. J., Menezes, R., and l. Su, T. (2010). Geostatistical inference under preferential sampling. *Journal of the Royal Statistical Society Series C - Applied Statistics*, 59:191–232.

Dunn, P. K. and Smith, G. K. (2005). Series evaluation of tweedie exponential dispersion model densities. *Stat. Comput.*, 15:267–280.

Fahrmeir, L. and Lang, S. (2001). Bayesian inference for generalized additive mixed models based on Markov random field priors. *J. R. Statist. Soc. C - Applied Statistics*, 50:201–220.

Gelfand, A., Banerjee, S., and Gamerman, D. (2005). Spatial process modelling for univariate and multivariate dynamic spatial data. *Environmetrics*, 16:465479.

Hilborn, R. and Ledbetter, M. (1985). Determinants of catching power in the british columbia salmon purse seine fleet. *Can. J. Fish. Aquat. Sci.*, 42:51–56.

Large, P. A., Diez, G., Drewery, J., Laurans, M., Pilling, G. M., Reid, D. G., Reinert, J., South, A. B., and Vinnichenko, V. I. (2010). Spatial and temporal distribution of spawning aggregations of blue ling (*molva dypterygia*) west and nortwest of the british isles. *ICES J. Mar. Sci.*, 67:494–501.

Lin, X. and Zhang, D. (1999). Inference in generalized additive mixed models by using smoothing splines. *J. R. Statist. Soc. B*, 61:381–400.

Lorance, P., Pawlowski, L., and Trenkel, V. M. (2010). Deriving blue ling abundance indices from industry haul by haul data. *ICES J. Mar. Sci.*, 67:1650–1658.

Mahevas, S., Sandon, Y., and Biseau, A. (2004). Quantification of annual variations in fishing power due to vessel characteristics: an application to the bottom-trawlers of south-brittany targeting anglerfish (*lophius budegassa* and *lophius piscatorius*). *ICES J. Mar. Sci.*, 61:71–83.

Maunder, M. N. and Punt, A. E. (2004). Standardizing catch and effort data: a review of recent approaches. *Fish. Res.*, 4:141–159.

Mikkonen, S., Rahikainen, M., Virtanen, J., Lehtonen, R., Kuikka, S., and Ahvonen, A. (2008). A linear mixed model with temoral covariance structures in modelling catch per unit effort of baltic herring. *ICES J. Mar. Sci.*, 65:1645–1654.

Piet, G. J. (2002). Using external information and gams to improve catch-at-age indices for north sea plaice and sole. *ICES J. Mar. Sci.*, 3:624–632.

Punt, A. E., Walker, T. I., Taylor, B. L., and Pribac, F. (2000). Standardization of catch and effort data in a spatially-structured shark fishery. *Fish. Res.*, 45:129–145.

Ribeiro Jr., P. and Diggle, P. (2001). geoR: a package for geostatistical analysis. *R-NEWS*, 1(2):15–18.

Silverman, B. W. (1985). Some aspects of the spline smoothing approach to nonparametric regression curve fitting. *J. R. Statist. Soc. B*, 47:1–52.

Strickland, C., Simpson, D., Turner, I., Denham, R., and Mengersen, K. (2011). Fast Bayesian analysis of spatial dynamic factor models for multitemporal remotely sensed imagery models for spatiotemporal data. *J. R. Statist. Soc. C - Applied Statistics*, 60:109–124.

Stroud, J., Muller, P., and Sanso, B. (2001). Dynamic models for spatiotemporal data. *J. R. Statist. Soc. B*, 63:673–689.

Tweedie, M. C. K. (1984). An index which distinguishes between some important exponential families. statistics: Applications and new directions. In Ghosh, J. K. and Roy, J., editors, *Proceedings of the Indian Statistical Institute Golden Jubilee International Conference*, pages 579–604. Calcutta: Indian Statistical Institute.

Wahba, G. (1983). Bayesian confidence intervals for the cross validated smoothing spline. *J. R. Statist. Soc. B*, 45:133–150.

Wood, S. N. (2004). Stable and efficient multiple smoothing parameter estimation for generalized additive models. *J. Am. Statist. Assoc.*, 99: 467:673–686.

Wood, S. N. (2006). *Generalized Additive Models. An Introduction with R.* Chapman & Hall/CRC, Boca Raton.

Wood, S. N. (2011). Fast stable restricted maximum likelihood and marginal likelihood estimation of semiparametric generalized linear models. *J. R. Statist. Soc. B*, 73(1):3–36.

Wood, S. N., Bravington, M. V., and Hedley, S. L. (2008). Soap film smoothing. *J. R. Statist. Soc. B*, 70(5):931–955.

Yanosky, J. D., Paciorek, C. J., Schwartz, J., Laden, F., and Suh, R. P. H. H. (2008). Spatio-temporal modeling of chronic pm10 exposure for the nurses' health study. *Atmospheric Environment*, 42:4047–4062.

Ye, Y. M. and Dennis, D. (2009). How reliable are the abundance indices derived from commercial catch-effort standardization? *Can. J. Fish. Aquat. Sci.*, 66:1169–1178.